

Soft Ball-Based Triboelectric–Electromagnetic Hybrid Nanogenerators for Wave Energy Harvesting

Yaokun Pang, Yuhui Fang, Jiaji Su, Huigang Wang, Yeqiang Tan,*
and Changyong (Chase) Cao*

Triboelectric nanogenerator (TENG) provides a new cost-effective strategy to harvest water wave energy due to the broad options of triboelectric materials and the high efficiency in low-frequency energy harvesting. Here, a new triboelectric–electromagnetic hybrid nanogenerator (TEHG) consisting of a soft ball-based triboelectric nanogenerator (SB-TENG) and an electromagnetic generator (EMG) is reported for harvesting wave energy. The soft balls are utilized as one triboelectric layer to increase the contact area with the copper electrodes. The critical parameters that may affect the energy harvesting performance of the SB-TENG are investigated, including the type of the filled liquids, the thickness of the silicone shell, the number of layers, and the added soft balls. Under an operating frequency of 1 Hz, the SB-TENG and the EMG can reach a maximum output peak power of 0.5 and 8.5 mW, respectively. The TEHG has been demonstrated to power dozens of light-emitting diodes and drives a digital temperature sensor to monitor the water temperature for an extended period. This study provides a new design and approach to improve the output performance of TENGs and presents an excellent prospect for building a self-powered water-sensing system driven by low-frequency water waves.

with other renewable energies, such as solar power and wind energy, ocean wave energy has the superior advantages of high power density, wide distribution, and low dependency on daytime, weather, and season.^[3–5] It is estimated that ocean waves can generate at least 8000 terawatt-hours of electricity per year if such energy can be harvested effectively.^[6,7] However, large-scale and efficient wave energy harvesting is still challenging due to the energy harvesters' low efficiency, high cost, and low frequency of ocean waves (<5 Hz).

Triboelectric nanogenerator (TENG), based on triboelectrification and electrostatic induction, has been extensively studied to harvest low-frequency mechanical energy,^[8–12] including wave energy. Previous studies have demonstrated that TENGs can effectively convert ocean wave energy into electrical output, with the merits of high output power, low cost, lightweight, ease of fabrication, and abundant choices of materials.^[13,14] Various

1. Introduction

Ocean wave energy is one of the most promising renewable energy sources for large-scale applications since more than 70% of the Earth's surface is covered by the ocean. It refers to ocean surface waves' kinetic and potential energy.^[1,2] Compared

TENGs with different structures have been proposed for wave energy harvesting, including the rolling ball structure,^[15,16] multilayered structure,^[17,18] grating structure,^[19] pendulum structure,^[20] and mass-spring structure.^[21,22] Among these designs, the rolling ball structure is the most fundamental and typical design for wave energy harvesting due to its high

Y. Pang, Y. Tan
State Key Laboratory of Bio-Fibers and Eco-Textiles
Collaborative Innovation Center of Marine Biobased Fiber and Ecological Textile Technology
Institute of Marine Biobased Materials
School of Materials Science and Engineering
Qingdao University
Qingdao 266071, China
E-mail: tanyeqiang@qdu.edu.cn

Y. Pang, J. Su, H. Wang, C. Cao
Laboratory for Soft Machines & Electronics
Department of Mechanical and Aerospace Engineering
Case Western Reserve University
Cleveland, OH 44106, USA
E-mail: ccao@case.edu

Y. Fang
4D Maker LLC
Okemos, MI 48864, USA

C. Cao
Department of Electrical
Computer, and Systems Engineering
Case Western Reserve University
Cleveland, OH 44106, USA

C. Cao
Advanced Platform Technology (APT)
Center Louis Stokes Cleveland VA Medical Center
Cleveland, OH 44106, USA

 The ORCID identification number(s) for the author(s) of this article can be found under <https://doi.org/10.1002/admt.202201246>.

DOI: 10.1002/admt.202201246

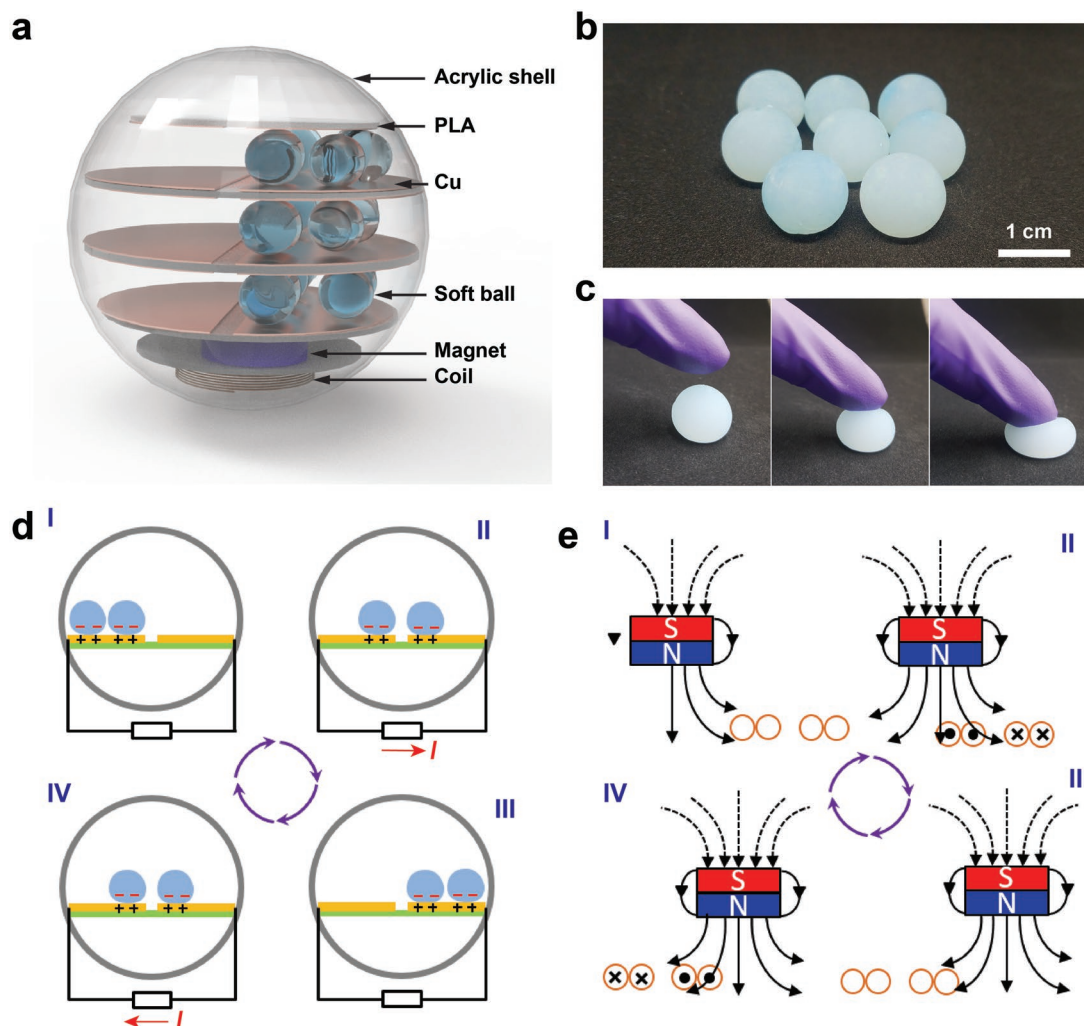


Figure 1. Prototype design and working principle of the triboelectric–electromagnetic hybrid generator (TEHG). a) Schematic illustration of the concept design for TEHG, consisting of soft ball-based TENGs (SB-TENG) and electromagnetic generator (EMG). Multiple soft balls are filled in the cavities formed by the layered structures in a spherical acrylic shell. b,c) Photographs of soft balls made of an Eco-flex 30 shell filled with liquid materials. The soft balls can generate a larger contact area with the copper electrodes. d) The schematic illustration of the working principle of the SB-TENG. e) The schematic illustration of the working principle of the EMG.

buoyancy and low resistance to water wave motions. However, these rolling ball-based TENGs using a single rolling ball inside a spherical shell have a small contact area and charge density, resulting in a low energy harvesting efficiency. One promising solution is to design a soft-contact mode TENG to increase the contact area and thereby improve the energy conversion efficiency.^[23–25] For example, Cheng et al. developed a soft-contact spherical TENG with a large contact area, resulting in a ten-fold enhancement of the maximum output charge compared to a hard PTFE ball.^[25] Xia et al. reported a multiple-frequency TENG based on the water balloon, which has a higher transferred charge than traditional TENG.^[26] However, the single large rolling ball has a low space utilization and small volumetric power density for a specific device. On the other hand, TENGs generate a high voltage but small current, thus a small output power. To increase the power output, combining the TENG and electromagnetic generator (EMG) will be a promising method for high-performance wave energy harvesting

because a hybrid system can fully use the captured motion energy in a broader operating bandwidth.^[27–30] Rotating sleeves and disks are the most commonly used structure in hybridized nanogenerators for harvesting mechanical energy.^[31–34] However, restricted by the mechanical structure, they can only harvest energy in a specific wave triggering direction, which is unsuitable for wave energy harvesting. In addition, the driven structures of some hybridized nanogenerators are based on a magnet ball,^[35,36] which is large and wastes the device's limited space. Thus, further investigation of advanced structural design for hybridized nanogenerators is still needed.

In this paper, we propose a triboelectric–electromagnetic hybrid nanogenerator (TEHG) based on soft balls to convert mechanical energy into electricity. As a proof-of-concept, three layers of SB-TENG units and an EMG unit are integrated into a spherical acrylic shell (Figure 1). For the TENG part, liquid/silicon soft balls were used to replace the traditional hard triboelectric material as the moving triboelectric layer that can

significantly increase the contact area to generate much more triboelectric charges. The EMG part composed of a magnet and copper coils is placed at the bottom of the device. Under the agitation of water waves, the soft balls and the magnet can simultaneously move back and forth in the shell. Thus, the water wave motions are converted into electricity. The key parameters that affect the energy harvesting performance of the TEHG are further systematically investigated, including the type of the liquid core materials, the thickness of the silicone rubber shell, and the number of layers of the soft balls. The output performance of the SB-TENG and EMG are systematically studied under various mechanical triggering conditions. We finally demonstrate that the new TEHG can lighten dozens of light-emitting diodes (LED) and power a digital temperature meter for environment monitoring.

2. Results and Discussion

2.1. Design and Working Principle of the TEHG

Figure 1a illustrates the structural design of the TEHG, which consists of two major parts: multilayered soft ball-based TENG and EMG. As a proof-of-concept, we fabricate a three-layers TENG unit by filling different numbers of soft balls (Figure 1b) into the cavity spaces between the adjacent circular polylactic acid (PLA) sheets. The circular PLA sheets are made as substrates by a 3D printer with the same thickness but different diameters. Two flat Cu conductive tapes are bonded onto the surface of the PLA sheets as the fixed triboelectric layers and conductive electrodes. The two electrodes are separated with a gap of ≈ 1 mm (Figure 1a). The soft balls made of silicone rubber (Ecoflex-30) have a diameter of ≈ 12 mm, and they can deform when pressed with a small force (Figure 1c). The soft ball has an internal cavity for filling liquid in so that the soft ball can generate more considerable deformation and contact area to improve the electricity generation of the TENG. The Ecoflex shell will be a negative tribo-material to form a pair with the copper layer. The detailed fabrication process of the soft ball can be found in the Experimental Section. To better observe the deformation and motion of the balls, we add a small amount of blue dye to the silicone rubber. Additionally, a copper coil with a circular pattern is embedded at the bottom of the acrylic shell, which has a dimension of $\varnothing 45$ mm \times 5 mm. A circular magnet with a diameter of 20 mm is placed on top of the bottom PLA sheet. This coil-magnet structure forms an EMG, which has the function of wave energy harvesting and lowers the device's center of gravity to prevent possible overturning. An acrylic sphere with a diameter of 120 mm is used as a shell and sealed well with waterproof glue to avoid potential water leakage, which may affect the generator's energy harvesting performance.

Figure 1d shows the working principle of the TENG unit, which is based on the conjugation of triboelectrification and electrostatic induction. When actuated by small wave agitations, the soft balls in the cavities of the device will freely move or roll back and forth between the two Cu electrodes, resulting in an alternating current in the external circuit. In brief, at the initial state (Figure 1d <II>), when the soft balls are in contact with

the left-hand Cu electrode, the soft balls are negatively charged. In contrast, the Cu electrode has the same number of positive charges in the saturated state due to its different abilities to attract electrons. At this moment, the tribo-charges will remain on the surfaces of the two triboelectric layers for an extended period. When the soft balls roll to the right-hand Cu electrode under the wave agitations, the equilibration of the electric field will be changed so that the free electrons flow from the right-hand electrode to the left-hand electrode, resulting in a forward current in the external load (Figure 1d <II>). When the soft balls leave the left-hand electrode and contact the right-hand electrode, all the positive charges on the left-hand electrode will be driven to the right-hand electrode (Figure 1d <III>). After that, the soft balls will move back to their original positions, and the free electrons flow back to the right-hand electrode, generating a reverse current in the external load (Figure 1d <IV>). Figure 1e illustrates the working mechanism of the EMG unit, which is based on electromagnetic induction. Under the wave agitation, the magnet slides right-left with the coil so that the coils cut magnetic induction lines, inducing an electromagnetic current. With the cyclic motions of the magnet, alternating electricity will be generated continuously in the coil.

2.2. Effect of the Materials and Structural Design on the Energy Harvesting Performance of SB-TENG

To make the soft balls highly elastic and flexible, we use silicone rubber to fabricate the ball's shells. The soft balls are expected to have a larger effective contact area with the electrodes so as to enhance the output performance of the TENG. However, it is found that the soft balls made of silicone rubber become sticky and generate a relatively large damping force at the interface, thus dramatically hindering the motions of the soft balls under the small agitations. Therefore, we stick polytetrafluoroethylene (PTFE) powders on the surface of the soft balls to reduce the damping force but simultaneously enhance contact electrification. As shown in **Figure 2a** and Video S1 (Supporting Information), the soft balls with PTFE powders are less sticky and can roll off fast on an inclined Cu surface.

In contrast, the soft balls without PTFE powders are very sticky, and the large damping force prevents it roll off from the inclined Cu surface. It should be noted that the PTFE powders are adsorbed on the surface of the soft balls relying on the highly sticky silicone rubber. We also added PTFE powders to the silicon rubber solution to obtain the composite material. However, it is found that this method has only a minimal effect on reducing the damping force and the higher content of PTFE powders decreases the flexibility of the soft ball. It is well known that PTFE is one of the most widely used triboelectric materials because of its high negativity in the triboelectric series. Figure 2b demonstrates that the TENG made of soft balls with PTFE powders can generate better output performance than that without PTFE powders under the same external agitations, attributing to the high tribo-negativity of PTFE.

Additionally, we examine the effect of liquid materials on the output performance of the SB-TENG. We inject a few kinds of liquids: tap water, deionized (DI) water, lubricating oil, and Ecoflex B, into the soft shell to compare the TENG's performance.

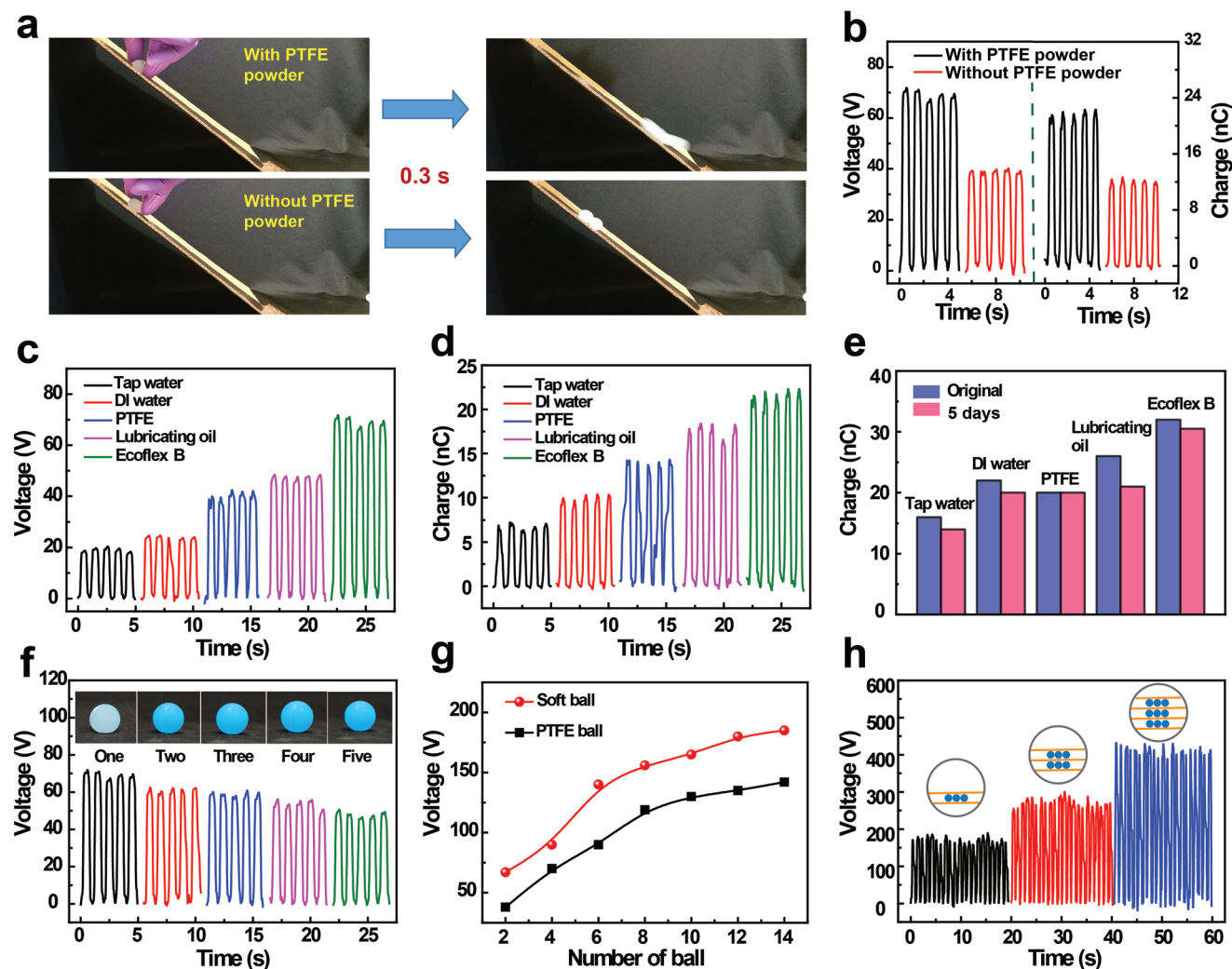


Figure 2. Effect of the critical factors of the SB-TENG on its energy harvesting performance. a) Photographs of the soft balls with and without PTFE powder rolling on a tilted Cu surface. b) Open-circuit voltage and transferred charge of the SB-TENG using two soft balls with and without PTFE powder. c) Variation of the induced voltage with the types of the filled liquid. d) Variation of the transferred charge with the types of the filled liquid. e) The stability of the SB-TENG's harvesting performance varies with the types of the filled liquids. f) Open-circuit voltage of the SB-TENG varies with the thickness of the soft balls. The insets show the photographs of the soft balls having different shell thicknesses. g) Variation of the open-circuit voltage of the TENG when using different number of soft balls and rigid PTFE balls. h) The open-circuit voltage of the SB-TENG as a function of the number of PLA layers.

The output performance of a TENG made of rigid PTFE balls is also studied for comparison. Figure 2c,d presents the influences of liquid type on the open-circuit voltage and short-circuit transferred charge of the SB-TENGs. It is obvious that the SB-TENGs filled with lubricating oil and Ecoflex B exhibit much higher output performance than those made of rigid PTFE balls. The SB-TENGs with Ecoflex B can generate a peak value of 70 V and 22 nC, respectively.

On the other hand, the SB-TENGs with tap water and DI water have a significantly lower output performance, about 30% or less of those made with Ecoflex B. The lower performance may be due to the screen effect of ions or charges in the water.^[37] As shown in Figure S1 (Supporting Information), the positive ions in the water can attract negative charges on the Ecoflex, which can interfere with the generation of contact electrification charges on the Cu electrode. Unlike water, Ecoflex B

and lubricating oil are liquid polymers without free ions so that they would not affect the contact electrification charge amount on the Cu electrode. To check the stability of the device, we test the short-circuit transferred charges of SB-TENGs made with different liquids at different times (0 h and five days) after fabrication. The test was conducted under the same testing conditions, and the number of samples increased to six. It can be seen from Figure 2e that the SB-TENGs made with lubricating oil have a considerable degradation of the output performance compared to those made with DI water, tap water, and Ecoflex B. The samples with Ecoflex B demonstrated little change after five days. This phenomenon may be attributed to the silicone rubber's low oil resistance and the oil's resultant leakage, especially when the thickness of the silicone rubber shell is skinny. Thus, in the following experiments, we will choose Ecoflex B as the filled liquid for new SB-TENGs.

In addition, we also investigate the influence of the shell thickness of the soft balls. As shown in Figure 2f, five different kinds of soft balls are made with different thicknesses by increasing the coating-curing times. It is observed that the output voltage of the SB-TENG decreases with the thickness of the silicone rubber shell. This difference should be due to the smaller contact area between the soft ball with a thicker shell and the electrodes. Although the thickness of the soft shell can be further reduced by adjusting the mixed ratio of the Ecoflex 30, its robustness will decrease, and the damping force will increase significantly.

We further compare the output performance of the SB-TENGs made of soft balls and PTFE balls. As shown in Figure 2g, the output performances of two kinds of TENGs have a similar increasing trend with the number of moving balls in the cavities. However, the increasing rate becomes smaller with more moving balls in the cavities. This change is attributed to the larger damping force and the smaller moving space in the device when having more balls. It can be found that the output voltage of the SB-TENG has been significantly improved compared to that of the rigid PTFE ball-based TENG. Figure 2h presents the output voltages of SB-TENGs with a different number of layers. Three layers can be integrated into the limited space of the SB-TENG unit. The measured output voltage of an SB-TENG with a single layer is around 180 V, and it can be enhanced to 430 V when having three layers in the device. This result indicates that a multilayered design can fully use the limited space in the device and significantly improve the output performance of the TENG.

2.3. Effect of the Excitation Mode and Conditions on the Energy Harvesting Performance of TEHG

Water waves in the ocean are very complex and may constantly change due to the uncertainty associated with many factors, such as wind, gravity, and planetary motion. To characterize the energy harvesting performance of the TEHG under different wave excitation conditions, we have categorized the motions into two basic movement modes, namely the translational mode and the swing mode (Figure 3a,f). A linear motor is used to simulate the two movement modes with assigned acceleration, speed, and displacement amplitude. The TEHG device is attached to a platform fixed on the linear motor for the translational mode to apply the vibration. With the excitation frequency varies from 0.5 to 2 Hz, the peak values of the output voltage and current generated by the SB-TENG increase to 450 V and 2 μ A, respectively (Figure 3b). The output voltage and current of the EMG have a similar variation trend, in which the voltage monotonically increases from 0.8 to 3 V and the current rises from 4 to 15 mA as the frequency increases from 0.5 to 2 Hz (Figure 3c). These results are in consistency with the Faraday's law, i.e., the voltage and current of the EMG are positively correlated with the moving velocity of the magnet. Figure 3d,e shows the effect of translational amplitude of the excitation on the output performance of TEHG. The output voltages and currents of the SB-TENG and the EMG are proportional to the translational amplitude at a frequency of

1.5 Hz. This variation should originate from the higher inertial acceleration of the soft balls and the magnet induced by the larger translational amplitude. Remarkably, less kinetic energy can be transferred to the soft balls and the magnet for a smaller translational amplitude and a lower frequency, thereby generating a much smaller electric output.

For the swing mode, as shown in Figure 3g, the peak output voltage and current of the SB-TENG at an orientation angle of 45° increase rapidly with the increasing swing frequency, from 285 V and 0.35 μ A at 0.25 Hz to 410 V and 1.3 μ A at 1.0 Hz, and then decrease at higher frequencies (>1.0 Hz). The initial increasing stage is attributed to the increased moving speed of the soft balls. However, when the swing frequency is higher than 1.0 Hz, the soft balls oscillate unstably to generate more collisions among the moving balls, resulting in uncompleted travels between the two Cu electrodes. On the other hand, the output performance of the EMG monotonically increases with the swing frequency (Figure 3h) due to the larger movement space and lower frictional force.

Figure 3i,j shows the TEHG's output performance variation with the orientation angle. Five different orientation angles, from 15° to 55°, were controlled under a constant swing frequency of 0.5 Hz. The output voltage and current of the SB-TENG gradually increase with the orientation angle, which is attributed to the more significant moving displacement of the soft balls under a larger orientation angle. The output voltage and current of the EMG first increase with the orientation angle increasing from 15° to 35° because the larger orientation angle generates a more significant moving displacement and a faster-moving speed of the magnet. However, when the orientation angle increases from 35° to 55°, the output performance of the EMG is kept nearly as constant due to the constraint of the shell on the continuous increase of the moving displacement and the magnet speed.

2.4. Evaluation of the New TEHG and Self-Powered Systems

The energy harvesting performance of TENGs is dependent on the external resistor loading. To optimize the energy harvesting performance, we have to investigate the impedance of the SB-TENG and the EMG. As shown in Figure 4a,b, the output voltages of the SB-TENG and the EMG increase with the increasing resistance loads while the output currents exhibit a reverse trend. It is found that when the external resistance is 700 M Ω , the SB-TENG reaches a peak power of 0.5 mW, while the EMG has a peak power of 8.6 mW at a load resistance of 180 Ω . The above results indicate that SB-TENG can be regarded as a current source with a high impedance, whereas the EMG is equal to a voltage source with a low impedance.^[28] According to the total volume of the device, the volumetric power density of the TEHG was calculated to be 10.1 W m⁻³. As shown in Figure S1 (Supporting Information), we list the volumetric power density of several triboelectric–electromagnetic hybrid nanogenerators from previous studies, and the TEHG exhibits the highest volumetric charge density.

Furthermore, the output performance of our device could be further enhanced by optimizing the structural design and

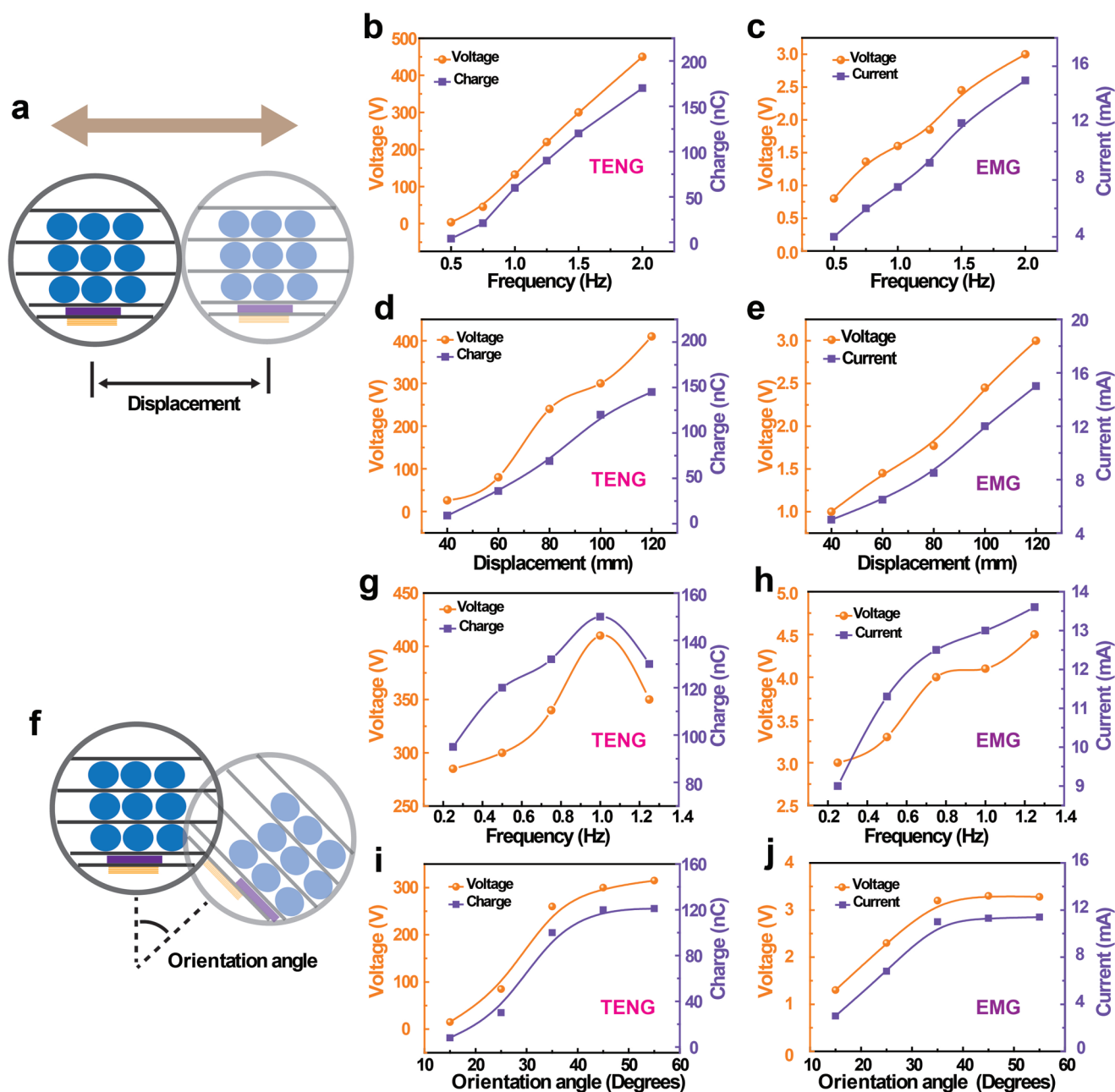


Figure 3. Energy harvesting performance of the TEHG under different excitation conditions. a) Schematic diagram of the translational mode. b) Output voltage of the SB-TENG and c) Output voltage of the EMG under different excitation frequencies. d) Output voltage of the SB-TENG and e) Output voltage of the EMG under different translational amplitudes. f) Schematic diagram of the swing mode. g) Output voltage of the SB-TENG and h) Output voltage of the EMG under different swing frequencies. i) Output voltage of the SB-TENG and j) Output voltage of the EMG under different orientation angles.

proper material selection. Figure 4c exhibits the charging voltage curves of a capacitor (10 μF) using an SB-TENG, an EMG, and a TEHG at a fixed charging time of 60 s and a working frequency of 1.0 Hz. Due to the relatively low output power and current, the charging rate of the SB-TENG is lower than that of the EMG. As for the EMG, the charging voltage quickly reaches about 2.1 V, and after that, the charging voltage increases slowly because of the low output voltage of EMG. By combining the advantages of the two parts, TEHG shows a much faster

charging rate and a higher charging voltage than the individual energy-harvesting unit SB-TENG or EMG. Figure 4d shows the charging voltage curves of a 10 μF capacitor by a TEHG under different frequencies. With the working frequency increasing, more energy can be harvested, and a higher charging voltage can be achieved. We also test the TEHG to charge different capacitors at the frequency of 1.0 Hz. As shown in Figure 4e, a TEHG can charge a smaller capacitor to reach a higher voltage at a faster charging rate during the same charging time.

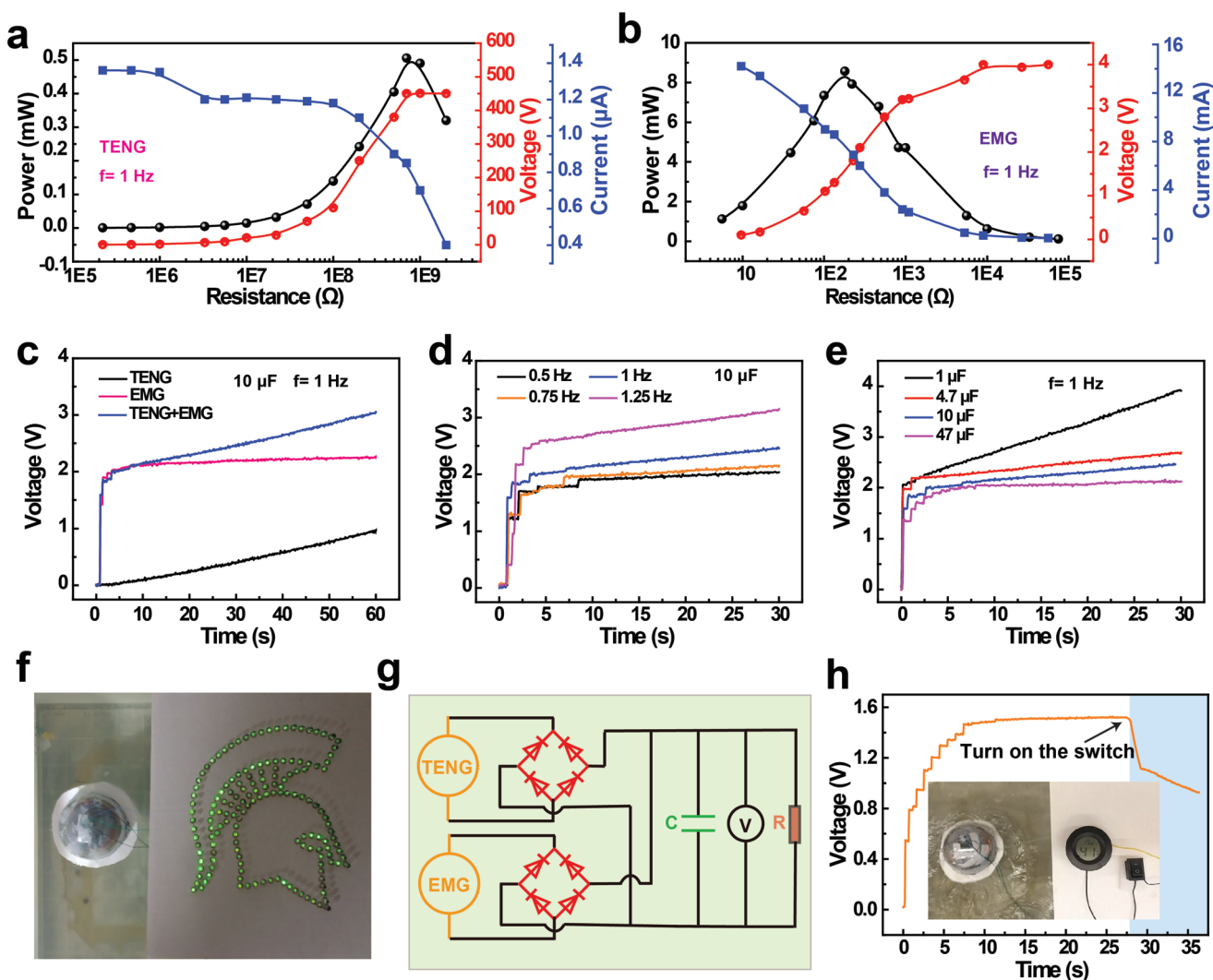


Figure 4. Energy harvesting performance the TEHG and a self-powered sensing system. a) Output power, current, and voltage of the SB-TENG vary with the external resistance loading. b) Output power, current, and voltage of the EMG vary with the external resistance loading. c) The charging curves of a capacitor ($10\ \mu\text{F}$) powered by an SB-TENG, EMG, and TEHG, respectively. d) The charging curves of different capacitors by a TEHG excited at $1.0\ \text{Hz}$. e) The charging curves of different capacitors by a TEHG excited at $1.0\ \text{Hz}$. f) The photographs of a TEHG lighten dozens of LEDs. g) Schematic diagram of the management circuit for a self-powered sensing system. h) The charging and discharging processes of a capacitor ($100\ \mu\text{F}$) to drive a temperature sensor by a TEHG. The insets show the photographs of the TEHG and the thermometer.

We place the TEHG device into a water tank to demonstrate its great potential in harvesting water wave energy (Figure 4f). Under the excitation of water waves, the TEHG can lighten dozens of light-emitting diodes (LEDs) (see Video S2 in the Supporting Information). We can integrate the TEHG with a rectifier, a storage capacitor, and two switches to form a self-powered electronics system, which can be used to power a sensor for long-term service (Figure 4g). The TEHG can charge a capacitor ($100\ \mu\text{F}$) in less than $10\ \text{s}$ by harvesting water wave energy (Figure 4h). When the charging voltage reaches $\approx 1.5\ \text{V}$, the thermometer powered by the capacitor is activated to measure the water temperature (see Video S3 in the Supporting Information). After discharging, the TENG can continue to charge it to the working voltage of $1.5\ \text{V}$ to power the sensor to work again.

3. Conclusions

We have proposed a new triboelectric–electromagnetic hybrid nanogenerator for water wave energy harvesting. The soft balls were designed as the moving triboelectric layer to increase the contact area. At the same time, a multilayered structure was adopted to fill more soft balls to utilize the device space fully. The energy harvesting performances of the SB-TENG and the EMG were investigated under different mechanical excitation conditions and configurations. With the optimal design, the SB-TENG and the EMG achieved a maximum output peak power of 0.5 and $8.5\ \text{mW}$, respectively, under an operating frequency of $1.0\ \text{Hz}$. Finally, we demonstrated a TEHG-based self-powered electronic system to drive a digital temperature sensor to measure the water temperature. This new design

provides an innovative and promising approach to effectively harvesting low-frequency water wave energy in the ocean for marine monitoring and electricity generation.

4. Experimental Section

Fabrication of the Soft Balls: The silicone rubber (Exoflex 00–30, Smooth-On, Inc.) was prepared by mixing the silicone base and precursor (Parts A and B) with a weight ratio of 1:1. As shown in Figure S2 (Supporting Information), a PTFE ball with a diameter of 12 mm was utilized as a mold and a fine needle was inserted into the PTFE ball. We dipped the PTFE ball into liquid silicone rubber and then placed it in an oven at 80 °C for 2 h. After that, the silicone shell was peeled off from the PTFE ball.

Finally, we injected liquid materials into the soft silicone shell through a small hole and sealed it with mixed silicone rubber. The sealed soft balls were placed in the oven for another 1 h for further use.

Fabrication of the TEHG: The circular PLA sheets are made as substrates by a 3D printer with the same thickness (1.5 mm). Two flat Cu conductive tapes are bonded onto the surface of the PLA sheets with a gap of ≈1 mm and connected with lead wires. Finally, the EMG, the soft ball, and the PLA sheets are integrated into an acrylic spherical shell with a diameter of 12 cm, as shown in Figure 1a.

Electrical Measurements of the TEHG: The open-circuit output voltage, short-circuit current and transferred charges of the SB-TENGs, the EMGs, and the TEHGs were measured by a current preamplifier (Keithley 6514 System Electrometer). A linear motor (LinMot MBT-37-120) was applied to drive the TEHG in the air and generate the water wave in a water tank. The software LabVIEW was programmed to acquire real-time control and data. All measured data were processed with MATLAB and Origin.

Supporting Information

Supporting Information is available from the Wiley Online Library or from the author.

Acknowledgements

This work was supported by USDA (2021-67021-33998), USDOT (693)K32050003CAAP), and the startup grant from Case Western Reserve University. Y.P. and Y.T. acknowledged the financial support of the Natural Science Foundation of Shandong Province (ZR2021JQ16, ZR2019YQ19).

Conflict of Interest

The authors declare no conflict of interest.

Data Availability Statement

The data that support the findings of this study are available from the corresponding author upon reasonable request.

Keywords

hybrid nanogenerators, self-powered sensing systems, triboelectric nanogenerators, wave energy harvesting

Received: July 30, 2022

Revised: September 24, 2022

Published online: January 25, 2023

- [1] T. Jeff, *Nature* **2014**, 508, 302.
- [2] O. Ellabban, H. Abu-Rub, F. Blaabjerg, *Renewable Sustainable Energy Rev.* **2014**, 39, 748.
- [3] I. R. Young, S. Zieger, A. V. Babanin, *Science* **2011**, 332, 451.
- [4] H. Wang, L. Xu, Z. Wang, *Nanoenergy Adv.* **2021**, 1, 32.
- [5] F. Shen, Z. Li, H. Guo, Z. Yang, H. Wu, M. Wang, J. Luo, S. Xie, Y. Peng, H. Pu, *Adv. Electron. Mater.* **2021**, 7, 2100277.
- [6] Z. Wang, *Nature* **2017**, 542, 159.
- [7] J. Falnes, *Mar. Corros. Offshore Struct., Pap. Symp.* **2007**, 20, 185.
- [8] F.-R. Fan, Z.-Q. Tian, Z. L. Wang, *Nano Energy* **2012**, 1, 328.
- [9] J. Luo, W. Gao, Z. L. Wang, *Adv. Mater.* **2021**, 33, 2004178.
- [10] G. Gu, G. Gu, J. Wang, X. Yao, J. Ju, G. Cheng, Z. Du, *Nano Energy* **2022**, 96, 107081.
- [11] Y. Pang, S. Chen, J. An, K. Wang, Y. Deng, A. Benard, N. Lajnef, C. Cao, *Adv. Funct. Mater.* **2020**, 30, 2003598.
- [12] K. Han, J. Luo, Y. Feng, L. Xu, W. Tang, Z. L. Wang, *Energy Environ. Sci.* **2020**, 13, 2450.
- [13] W. Li, Y. Pei, C. Zhang, A. G. P. Kottapalli, *Nano Energy* **2021**, 84, 105865.
- [14] Z. Ren, X. Liang, D. Liu, X. Li, J. Ping, Z. Wang, Z. L. Wang, *Adv. Energy Mater.* **2021**, 11, 2101116.
- [15] Y. Pang, S. Chen, Y. Chu, Z. L. Wang, C. Cao, *Nano Energy* **2019**, 66, 104131.
- [16] Z. Wu, H. Guo, W. Ding, Y.-C. Wang, L. Zhang, Z. L. Wang, *ACS Nano* **2019**, 13, 2349.
- [17] L. Xu, Y. Pang, C. Zhang, T. Jiang, X. Chen, J. Luo, W. Tang, X. Cao, Z. L. Wang, *Nano Energy* **2017**, 31, 351.
- [18] L. Liu, X. Yang, L. Zhao, H. Hong, H. Cui, J. Duan, Q. Yang, Q. Tang, *ACS Nano* **2021**, 15, 9412.
- [19] Y. Bai, L. Xu, C. He, L. Zhu, X. Yang, T. Jiang, J. Nie, W. Zhong, Z. L. Wang, *Nano Energy* **2019**, 66, 104117.
- [20] P. Rui, W. Zhang, Y. Zhong, X. Wei, Y. Guo, S. Shi, Y. Liao, J. Cheng, P. Wang, *Nano Energy* **2020**, 74, 104937.
- [21] Y. Sun, F. Zheng, X. Wei, Y. Shi, R. Li, B. Wang, L. Wang, Z. Wu, Z. L. Wang, *ACS Appl. Mater. Interfaces* **2022**, 14, 15187.
- [22] T. Jiang, Y. Yao, L. Xu, L. Zhang, T. Xiao, Z. L. Wang, *Nano Energy* **2017**, 31, 560.
- [23] Z. Lin, B. Zhang, Y. Xie, Z. Wu, J. Yang, Z. L. Wang, *Adv. Funct. Mater.* **2021**, 31, 2105237.
- [24] D. Guan, X. Cong, J. Li, H. Shen, C. Zhang, J. Gong, *Nano Energy* **2021**, 87, 106186.
- [25] P. Cheng, H. Guo, Z. Wen, C. Zhang, X. Yin, X. Li, D. Liu, W. Song, X. Sun, J. Wang, Z. L. Wang, *Nano Energy* **2019**, 57, 432.
- [26] K. Xia, J. Fu, Z. Xu, *Adv. Energy Mater.* **2020**, 10, 2000426.
- [27] Y. Pang, Y. Cao, M. Derakhshani, Y. Fang, Z. L. Wang, C. Cao, *Matter* **2021**, 4, 116.
- [28] C. Zhang, W. Tang, C. Han, F. Fan, Z. L. Wang, *Adv. Mater.* **2014**, 26, 3580.
- [29] L. Liu, Q. Shi, C. Lee, *Nano Res.* **2021**, 14, 4227.
- [30] Z. Li, C. Wang, F. Ling, L. Wang, R. Bai, Q. Chen, H. Yuan, Y. Yu, Y. Tan, *Adv. Mater.* **2022**, 34, 2204214.
- [31] R. Cao, T. Zhou, B. Wang, Y. Yin, Z. Yuan, C. Li, Z. L. Wang, *ACS Nano* **2017**, 11, 8370.
- [32] Y. Chen, Y. Cheng, Y. Jie, X. Cao, N. Wang, Z. L. Wang, *Energy Environ. Sci.* **2019**, 12, 2678.
- [33] H. Yang, W. Liu, Y. Xi, M. Lai, H. Guo, G. Liu, M. Wang, T. Li, X. Ji, X. Li, *Nano Energy* **2018**, 47, 539.
- [34] H. Yang, M. Wang, M. Deng, H. Guo, W. Zhang, H. Yang, Y. Xi, X. Li, C. Hu, Z. Wang, *Nano Energy* **2019**, 56, 300.
- [35] J. He, X. Fan, J. Mu, C. Wang, J. Qian, X. Li, X. Hou, W. Geng, X. Wang, X. Chou, *Energy* **2020**, 194, 116871.
- [36] Z. Wu, H. Guo, W. Ding, Y.-C. Wang, L. Zhang, Z. L. Wang, *ACS Nano* **2019**, 13, 2349.
- [37] J. Nie, Z. Ren, L. Xu, S. Lin, F. Zhan, X. Chen, Z. L. Wang, *Adv. Mater.* **2020**, 32, 1905696.